Controllable nucleation and propagation of topological magnetic solitons in CoFeB/Ru ferrimagnetic superlattices

A. Fernández-Pacheco,* D. Petit, R. Mansell, R. Lavrijsen, J. H. Lee, and R. P. Cowburn

Thin Film Magnetism Group, Cavendish Laboratory, University of Cambridge, JJ Thompson Avenue, CB3 0HE, Cambridge, United Kingdom

(Received 27 April 2012; revised manuscript received 30 August 2012; published 17 September 2012)

We control the nucleation and propagation of topological magnetic solitons in synthetic ferrimagnetic $(CoFeB/Ru)_N$ superlattices ($N = 6$). This is achieved by carefully tuning the anisotropy and thickness of one of the edge layers, making it different from the other layers of the superlattice. Sharp solitons can be nucleated at one edge of the system, then unidirectionally propagated using external magnetic fields. Experimental results are modeled with macrospin simulations. We present a numerical phase diagram which maps the general behavior for the nucleation and propagation of solitons in ferrimagnets.

DOI: 10.1103/PhysRevB.86.104422 PACS number(s): 75.70.−i, 75.25.−j, 75.50.Gg, 75.60.Ch

Domain walls in ferromagnetic nanowires have been the focus of extensive research activity during the last few years because of technological applications for magnetic storage and logic,[1,2] as well as for the interesting physics involved.[3–5] These studies are based on the perfect control achievable for the nucleation and propagation of domain walls along nanowires. Some works have envisaged extending this area of research to three dimensions (3D).[1,6] However, great complexity exists in the fabrication of these 3D nanostructures. In synthetic antiferromagnets (SAFs) the effects caused by uncompensated edge layers have been extensively studied in the past.[7–12] It has been shown that superlattices (SLs) with a large number of layers, $N \approx 20$,[7,8,12] present inhomogeneous states during the surface spin-flop transition, consisting of a few layers flopped towards the field and the rest remaining antiparallel. Upon increasing the applied magnetic field, the flopped layers move into the bulk of the SL, separating the two possible antiphases. The aforementioned spin frustration, analogous to a domain wall in a nanowire, is a topological (kink) magnetic soliton.[10] The large potential of using antiferromagnets as active components in spintronic devices has been recently shown.[13,14] The use of SAFs for this purpose is very convenient since the intra- and interlayer properties can be finely tuned. In order to use solitons in SAFs as mobile objects, the control of the nucleation, direction of propagation, and extension of that type of spin texture is required. In this paper we study $(CoFeB/Ru)_N$ synthetic ferrimagnetic SLs ($N = 6$), with the coupling/anisotropy ratio between the top five layers chosen to be 1.75, and the anisotropy and thickness of one of the edge layers varied from the others. This small asymmetry in the SL makes it possible to control the nucleation of sharp solitons, which can be unidirectionally propagated along the system by means of magnetic field sequences. We explore the range of parameters where these nucleation and propagation processes are possible.

A SL, formed by N antiferromagnetically coupled ferromagnetic layers, is shown in Fig. 1(a). For an external field H applied along the easy axis direction, the total energy per unit area (u) is given by

$$u = M_s \left\{ \sum_{i=1}^{N} t_i \left(\frac{1}{2} H_{ui} \sin^2 \theta_i - H \cos \theta_i \right) + \sum_{i=1}^{N-1} \left[t_i H_{Ji} \cos (\theta_{i+1} - \theta_i) \right] \right\}. \quad (1)$$

Where the index i refers to the layer number, θ_i is the angle formed by the magnetization with the easy axis, t_i is the layer thickness, $H_{ui} = 2K_i/M_s$ is the anisotropy field, with K_i the anisotropy energy per unit volume, M_s is the saturation magnetization of the films, and $H_{Ji} = J/(M_s t_i)$ is the coupling field between layers, with J the coupling energy per unit area. For the ferrimagnets of this work, the properties of layer 1 are different from the rest of the layers [see Fig. 1(a)]: J is constant, but t_1 and K_1 are altered. Thus, calling H_u and H_J the anisotropy and coupling fields for $i > 1$, $H_{u1} \neq H_u$ and $H_{J1} = (t/t_1)H_J$.

The samples were grown by magnetron sputtering, with the following structure, from bottom to top: Ta(2–5 nm)/CoFeB(t_1)/Ru(3.4 nm)/[CoFeB(5 nm)/Ru(3.4 nm)]$_5$/Ta(5 nm). All CoFeB layers are antiferromagnetically coupled by Ru via RKKY interactions. The Ru thickness corresponds to the third antiferromagnetic peak,[15] with $J = -19.2$ merg/cm^2, that is, $H_J = -35$ Oe. An external magnetic field was applied during the growth to create a well-defined uniaxial anisotropy direction in the ferromagnetic layers.[16] The strength of the anisotropy of layer 1 was varied by changing its thickness[17] and the thickness of the seedlayer.[16] H_{ui} was determined by measuring the hard-axis saturation field of the corresponding single layer. All the upper $t = 5$ nm films ($i > 1$) present well-defined in-plane easy axes, with $H_u = 20$–25 Oe. The layers were investigated under applied magnetic fields by a longitudinal magneto-optical Kerr effect, with a 5 μm laser spot, complemented by vibrating-sample-magnetometer (VSM) measurements. The system was modeled using macrospin simulations, where each layer is represented as one single spin.[7,9,18] The energy of the system [Eq. (1)] was minimized using a Monte Carlo method. In order to obtain good agreement between the experiments and simulations, H_u and H_J for each layer were allowed to vary by a maximum of 20% from the values previously detailed.

Figure 1(b) shows the easy axis Kerr response of a synthetic ferrimagnet with $N = 6$, $t_1 = 15$ nm $= 3t$, and $H_{u1} = 36$ Oe $= 1.75 H_u$. Circles are experimental Kerr data, and the blue line is the Kerr signal obtained from simulations. The magnetization

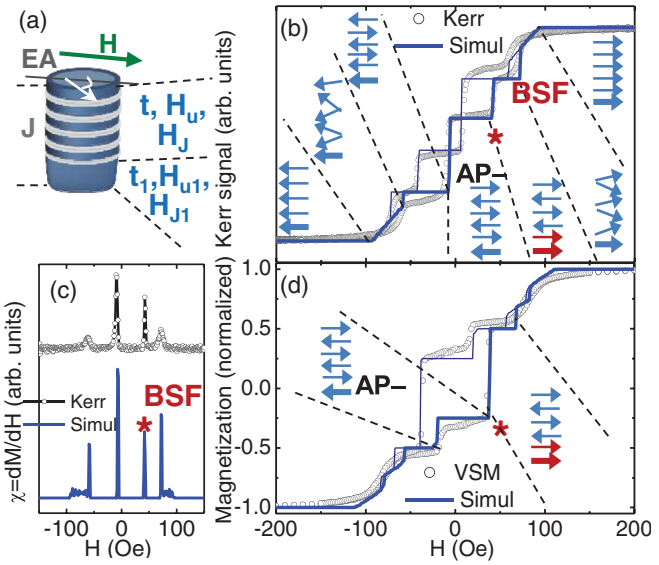

FIG. 1. (Color online) (a) Sketch of the investigated $(CoFeB/Ru)_6$ SL. (b) Kerr and (d) VSM signal as a function of the applied magnetic field for a SL with $t_1 = 15$ nm and $H_{u1} = 36$ Oe. (c) Magnetic susceptibility for the negative-to-positive field branch, from Kerr data and simulations.

of the layers during a half field cycle (thick line), extracted from the simulations, is shown by arrows. The angle formed by the arrows with the horizontal is the one formed by the magnetization with the easy axis, both in the plane of the films. The magnetic susceptibility $\chi = dM/dH$ during that half cycle is shown in Fig. 1(c). Coming from negative saturation, the spins are in an antiparallel (AP) state at remanence, as expected, since $H_J > H_u$. Of the two possible AP states, Zeeman energy favors that the (thick) bottom layer is pointing leftwards (AP–). Defining the parameter $\Phi_i = (-1)^{i-1} \cos\theta_i$, AP– has $\Phi = -1$ for all layers. On increasing the field, the next transition corresponds to the switching of layer 1 at H_1^* marked with an asterisk. This configuration, with the two bottom layers aligned in parallel [arrows marked in red in Fig. 1(b)], and the rest staying AP, extends for a few tens of Oersted. In this case, $\Phi_1 = +1$ for the bottom layer, contrary to the rest of the SL. For higher fields, the upper layers evolve towards saturation via flopping (marked in the figure with BSF). Figure 1(d) shows the normalized magnetization of this sample (circles), in good agreement with simulations (line). The small differences between macrospin simulations and VSM data observed for low fields may be due to some defects within the area probed by VSM, $\approx$1 cm^2, or to the presence of domains. For this range of fields, Kerr loops show a better agreement between the two signals, suggesting that if domains are formed, they are larger than the laser spot.

By minimizing Eq. (1) the switching field of a layer i, coming from remanence, is given by[18]

$$H_i^* = \sqrt{2H_{Ji}H_{ui} + H_{ui}^2}. \quad (2)$$

Previous works[7–12] have studied SLs with all identical layers (denominated hereafter homogeneous SAFs). In homogeneous SAFs with even N, one of the two equivalent surface layers ($i = 1$ or N), coupled by H_J, is opposite to the field. Substituting values for that layer into Eq. (2) gives the surface spin-flop (SSF) field $H_{SSF} = (2H_J H_u + H_u^2)^{1/2}$. On the contrary, bulk layers ($1 < i < N$) are coupled by $2H_J$, giving the bulk spin-flop (BSF) field $H_{BSF} = (4H_J H_u + H_u^2)^{1/2}$. This difference between H_{SSF} and H_{BSF} allows the spins at the edges to reverse first. In homogeneous SAFs formed by a large N,[7,11,12] 2–3 layers flop at one of the edges. These flopped spins move towards the center of the stack as H is increased, forming a soliton separating the two antiphase domains ($\Phi = \pm 1$). As H increases further, the soliton broadens until the BSF transition, where the SL reaches a homogeneous flopped state. Here, since we alter the properties of the bottom layer, the SL does not undergo a conventional SSF. Equation (2) for layer 1 yields a switching field $H_1^* \approx 45$ Oe, different from the SSF value for an edge layer in an equivalent homogeneous SAF, $H_{SSF} \approx 50$ Oe. More importantly, as the field is increased, the magnetic configuration of the system does not change until the BSF transition, at $H_{BSF} \approx 65$ Oe (same value as in a homogeneous SAF). This behavior is a consequence of the value of H_{J1}/H_{u1}, which is about 4 times smaller than H_J/H_u. This is also manifested during the BSF, where the canting of the bottom spin is smaller than for the rest of the layers.

The evolution of the SL after H_1^* is explored in Fig. 2 by minor loops. Figures 2(a) and 2(c) are experimental Kerr data for two different ferrimagnets, with $N = 6$. In both cases, the structure of the stack is identical for $i > 1$ layers: $t = 5$ nm, $H_u = 20$ Oe, whereas the properties of the bottom layer are different. In Fig. 2(a) $t_1 = 15$ nm and $H_{u1} = 36$ Oe, and in Fig. 2(c) $t_1 = 10$ nm and $H_{u1} = 15$ Oe. $H_J = -35$ Oe is constant along the whole stack. Figures 2(b) and 2(d) are the respective Kerr simulations for the two samples, in good agreement with the experimental results. The black line is the negative-to-positive branch of the major loop, and the blue line is a minor loop, going from the initial (I) to the final (F) state. In both cases, from negative saturation, an AP– ($\Phi_i = -1$) state is formed at remanence (I), followed by the switching of the bottom layer at H_1^*. As discussed before, at that field

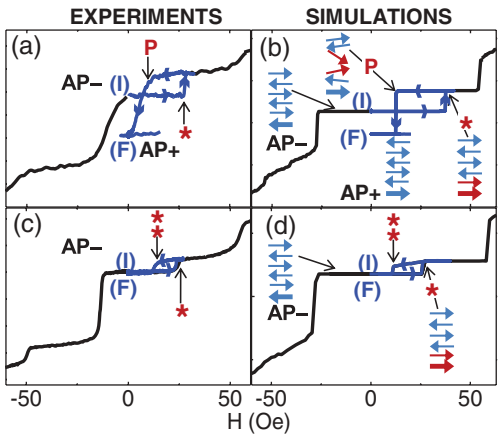

FIG. 2. (Color online) (a) and (c) Experimental Kerr data, (b) and (d) simulated Kerr for $N = 6$. (a) and (b) For $t_1 = 15$ nm, $H_{u1} = 36$ Oe, a soliton is nucleated and propagated. (c) and (d) For $t_1 = 10$ nm, $H_{u1} = 15$ Oe the bottom layer switches back, returning to AP– at remanence.

$\Phi_1 = +1$ and Φ_i $(i > 1) = -1$. If the field is now reversed, a substantial difference between Figs. 2(a) and 2(c) is observed. In Fig. 2(a), from H_1^* to (F), the top five layers reverse, at a positive field, marked with P in the figure, $H_P \approx +12$ Oe. As a result, the AP+ configuration is formed at the second remanent state (F), that is, $\Phi = +1$ for all layers. A different situation occurs in Fig. 2(c). When the field reverses from H_1^*, the bottom layer switches back at a field marked with **, with the upper layers staying in the same configuration: The (F) state is AP−, the same as in (I).

Coming from positive saturation, the field necessary to reverse layer 1 back is[18]

$$H_1^{**} = \frac{2|H_{J1}| - H_{u1}}{\sqrt{1 + 2|H_{J1}|/H_{u1}}}. \quad (3)$$

In the case shown in Fig. 2(a), Eq. (3) gives $H_1^{**} = -9$ Oe, which is lower than H_P, the field that reverses the rest of the layers. On the contrary, in Fig. 2(c), due to a lower anisotropy and higher coupling, $H_1^{**} = +11$ Oe, which is larger than H_P in this SL. In Fig. 2(b) simulations show how at H_P the upper layers are sequentially reversed upon decreasing H, due to the coupling between them. The transition from $\Phi = +1$ to $\Phi = -1$ moves upwards, that is, a soliton is propagated along the SL. The initial switching of the bottom layer creates a topologically locked state. The only way to erase it and return to an AP state at remanence is to propagate a soliton upwards through the whole stack, ending in the contrary AP state (Φ goes from -1 to $+1$). Figure 2(b) shows a snapshot of the simulations when the soliton has reached the middle of the stack. Analogously to a domain wall in a nanowire, the soliton width depends on the coupling-anisotropy ratio. As $|H_J|/H_u > |H_{J1}|/H_{u1}$ and $H < H_1^*$, the soliton, initially sharp when it was nucleated at the edge, broadens in the bulk, with the angle formed by the layers at the center of the soliton with the easy axis larger than when it was at the bottom. The neighboring spins are also slightly rotated from the easy axis, by a smaller amount for the bottom spins than for the top ones. On the contrary, in Figs. 2(c) and 2(d) the bottom layer reverses back, ending with $\Phi = -1$, as before.

The two cases shown before exemplify how sensitive the mechanisms for nucleation and propagation of solitons are to the ratio between the properties of layer 1 and the upper ones; in other words, how ferrimagnetic the SL is. This is generally explored via simulations in Fig. 3, with t_1/t being varied from 0.8 to 4, and H_{u1}/H_u from 0.2 to 3. The coupling between layers is fixed to the same value as before: $H_J = -35$ Oe. The bottom part of the figure shows sketches of the layers for the three states investigated by minor loops: At the first remanent state coming from negative fields (I), at the positive switching field where the arrangement existing at (I) changes, and at the second remanent state by decreasing H (F). Three main regions are observed: Soliton-nucleation-and-propagation (R1), edge-layer-switching (R2), and BSF (R3). The situations modeled before in Figs. 2(b) and 2(d) correspond to R1 and R2, respectively. In both areas layer 1 reverses separately from the rest of the SL at H_1^*. In R1, $H_P > H_1^{**}$, and a soliton is propagated upwards upon decreasing the field; in R2, $H_P < H_1^{**}$, and the bottom layer reverses instead. R1 only exists for $t_1/t > 1.5$. As t_1/t is increased from that critical value, R1 is expanded to the detriment of R2. This is

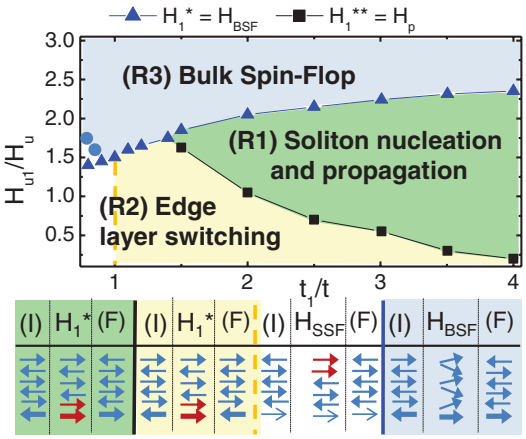

FIG. 3. (Color online) (Top) Magnetization reversal phase diagram as a function of anisotropy field and thickness ratios between the first and the rest of the layers, obtained from simulations for an $N = 6$, $H_J = -35$ Oe SL. The response of the system is studied for minor loops as in Fig. 2. Three main regions are observed. In R1, controllable nucleation and propagation of solitons along the SL is achieved. (Bottom) Magnetization at the three investigated states, for each region of the diagram.

because, in spite of a low H_{u1}/H_u, the ever thicker bottom layer will stay positive after H_1^* when returning to zero fields, leading to the formation of a mobile soliton since switching to the negative direction would have a too high Zeeman energy cost. For R3, H_{u1}/H_u becomes higher, making $H_1^* > H_{\rm BSF}$. In this region, the whole system transits directly from AP− to a BSF state at $H_{\rm BSF}$. The SSF is blocked, with the $N = 6$ system effectively behaving as a SL with an odd number of layers.

The case $t_1/t = 1$ requires special attention since previous literature has mainly focused on this type of system. If $H_{u1}/H_u = 1$, the system is symmetric, and the SSF initiates from whichever layer was opposite to the field at (I). By varying H_{u1}/H_u, the state present at remanence (I) is controlled: If $H_{u1}/H_u < 1$, (I) will be AP+, and the top surface flops at $H_{\rm SSF}$, whereas if $1 < H_{u1}/H_u < 1.5$, (I) will be AP−, and therefore the bottom film switches at H_1^*. However, these spin arrangements are always reversed when the field is reversed (R2). When $H_{u1}/H_u > 1.5$, the layers directly transit into a BSF state (R3). Thus, the presence of a thicker edge layer is essential for a successful nucleation and propagation of solitons using the mechanisms explained here. In general, in a homogeneous SAF where the nucleation of a soliton occurs via a SSF at the bottom surface, the only possibility for upwards propagation is if the soliton moves beyond the center of the stack. For that, a field very close to $H_{\rm BSF}$ is necessary, which greatly increases the soliton width.[7,9,11] Moreover, the exact configuration of the SL near BSF is very sensitive to small variations in the layer properties. On the contrary, the process shown here for R1 is robust: The soliton extension is well controlled since the maximum field needed is $\approx H_1^*$, the propagation direction is well defined, and it does not depend on N as long as it is even.

For the last region of the diagram, when $t_1/t < 1$, let us discuss the particular case $t_1/t = 0.8$. When $H_{u1}/H_u < 1.7$, the state at (I) is AP+: the top layer will switch at $H_{\rm SSF}$, reversing back into AP− as H is reversed. That is the behavior

of the whole white area inside R2, including a small region above the $H_1^* = H_{BSF}$ line (triangles): An AP+ state at (I) will always transit to a SSF state. On the contrary, when $H_{u1}/H_u > 1.7$, the bottom layer has high enough anisotropy for the SL to end into AP− at (I). However, for this ratio, $H_1^* > H_{BSF}$, and the system directly goes to a BSF state.

Figure 3 was calculated for $|H_J|/H_u = 1.75$, the same as experimentally. For this value, a wide R1 region is found for the formation of mobile solitons in SLs with $N = 6$. Nevertheless, previous literature has focused on antiferromagnetic SLs with much higher ratios: Typically above 10 for GMR[19] or SSF phenomena studies.[7,11] We have explored the reversal behavior of an $N = 6$ system for one point of the diagram ($H_{u1}/H_u = 1.5$, $t_1/t = 3$), as a function of $|H_J|/H_u$. Under those conditions, R1 holds as long as $|H_J|/H_u < 2.25$. For higher values, however, the solitons nucleated at the bottom layer are not stable in the system, being immediately expelled up the stack at H_1^*. The coupling/anisotropy ratio of the SL is therefore essential for the formation of stable solitons. Additional simulations (not shown here) indicate that the stability of a soliton inside the SL is largely dependent on N.

In summary, we have studied the magnetization reversal in CoFeB/Ru synthetic ferrimagnetic superlattices. By tuning carefully the properties of the bottom layer with respect to the others, the reversal behavior of the system is controlled. Topological magnetic solitons can be nucleated at the edge of the system, which are unidirectionally propagated along the superlattice using external magnetic fields. The mechanism shown here for the generation and motion of localized magnetic solitons in synthetic ferrimagnets is very robust if the appropriate coupling/anisotropy ratio is chosen. The control on the nucleation and propagation of artificial spin textures in synthetic systems is relevant from both a fundamental point of view, as well as for spintronic applications.

A.F.-P. acknowledges support by a Marie Curie IEF within the 7th European Community Framework Programme No. 251698: 3DMAGNANOW. R.L. acknowledges support from the Netherlands Organization for Scientific Research and Marie Curie Cofund Action (NWO-Rubicon 680-50-1024). We acknowledge research funding from the European Community under the Seventh Framework Programme Contract No. 247368: 3SPIN.

*Corresponding author: af457@cam.ac.uk

[1] S. S. P. Parkin, M. Hayashi, and L. Thomas, Science **320**, 190 (2008).
[2] D. A. Alwood, G. Xiong, C. C. Faulkner, D. Atkinson, D. Petit, and R. P. Cowburn, Science **309**, 1688 (2005).
[3] L. Heyne, M. Kläui, D. Backes, T. A. Moore, S. Krzyk, U. Rüdiger, L. J. Heyderman, A. Fraile Rodríguez, F. Nolting, T. O. Mentes, M. A. Niño, A. Locatelli, K. Kirsch, and R. Mattheis, Phys. Rev. Lett. **100**, 066603 (2008).
[4] S. Ladak, D. E. Read, G. K. Perkins, L. F. Cohen, and W. R. Branford, Nat. Phys. **6**, 359 (2010).
[5] T. Koyama, D. Chiba, K. Ueda, K. Kondou, H. Tanigawa, S. Fukami, T. Suzuki, N. Ohshima, N. Ishiwata, Y. Nakatani, K. Kobayashi, and T. Ono, Nat. Mater. **10**, 194 (2011).
[6] R. P. Cowburn and D. Allwood, U.S. Patent No. 0047156 A1 (1 March 2007).
[7] R. W. Wang, D. L. Mills, E. E. Fullerton, J. E. Mattson, and S. D. Bader, Phys. Rev. Lett. **72**, 920 (1994).
[8] A. S. Carriço, R. E. Camley, and R. L. Stamps, Phys. Rev. B **50**, 13453 (1994).
[9] S. Rakhmanova, D. L. Mills, and E. E. Fullerton, Phys. Rev. B **57**, 476 (1998).
[10] C. Micheletti, R. B. Griffiths, and J. M. Yeomans, Phys. Rev. B **59**, 6239 (1999).
[11] S. G. E. te Velthuis, J. S. Jiang, S. D. Bader, and G. P. Felcher, Phys. Rev. Lett. **89**, 127203 (2002).
[12] J. Meersschaut, C. Labbe, F. M. Almeida, J. S. Jiang, J. Pearson, U. Welp, M. Gierlings, H. Maletta, and S. D. Bader, Phys. Rev. B **73**, 144428 (2006).
[13] B. G. Park, J. Wunderlich, X. Martí, V. Holý, Y. Kurosaki, M. Yamada, H. Yamamoto, A. Nishide, J. Hayakawa, H. Takahashi, A. B. Shick, and T. Jungwirth, Nat. Mater. **10**, 347 (2011).
[14] S. Loth, S. Baumann, C. P. Lutz, D. M. Eigler, and A. J. Heinrich, Science **335**, 196 (2012).
[15] A. Hashimoto, S. Saito, K. Omori, H. Takashima, T. Ueno, and M. Takashi, Appl. Phys. Lett. **89**, 032511 (2006).
[16] S. Kong, T. Okamoto, and S. Nakagawa, J. Appl. Phys. **93**, 6778 (2003).
[17] R. Lavrijsen, P. V. Paluskar, C. T. J. Loermans, P. A. van Kruisbergen, J. T. Kohlhepp, H. J. M. Swagten, and B. Koopmans, J. Appl. Phys. **109**, 093905 (2011).
[18] B. Dieny, J. P. Gavigan, and J. P. Rebouillat, J. Phys. Condens. Matt. **2**, 159 (1990).
[19] S. S. P. Parkin, Phys. Rev. Lett. **67**, 3598 (1991).